Flow Past a Two-Dimensional Body : Motion of Fluid Particles (流体力学における非定常問題)

AUTHOR(S):

HORIUCHI, KIYOSHI; ONO, KIYOAKI; KUWAHARA, KUNIO

CITATION:

HORIUCHI, KIYOSHI ...[et al]. Flow Past a Two-Dimensional Body : Motion of Fluid Particles (流体力学における非定常問題). 数理解析研究所講究録 1980, 393: 166-183

ISSUE DATE:

1980-08

URL:

http://hdl.handle.net/2433/104969

数理解析研究所講究録
393巻 1980年 166-183

Flow past a Two-Dimensional Body; Motion of Fluid Particles

Kiyosi Horiuti, Kiyoaki Ono*, Kunio Kuwahara

Dept. Applied Physics, Univ. Tokyo.
* Coll. Sci. & Tech., Nihon Univ.

The flow fields around an elliptic cylinder and around an oscillating airfoil were analized numerically using the discrete-vortex approximation; the boundary layer along the body surface is divided into a finite number of elements and replaced by the same number of the corresponding vortex filaments at each time step, the circulations of which are determined to be equal to those of the elements. Some experimental measurements are also carried out to see the validity of the discrete-vortex method. This paper consists of two parts. In Part I, flow around an elliptic cylinder with the thickness ratio of 0.5 at an angle of attack of 45°, and 90°, having started impulsively, was investigated. In Part II, the flow around an oscillating airfoil under pitching and/or heaving motion was studied, where the maximun angle of attack during oscillation was taken to be larger than the static stall one.

PART I ELLIPTIC CYLINDER

1. Introduction

It is a familiar phenomenon that an obstacle sheds series of vortices alternatively into the wake, which form a vortex street. In order to solve the full Navier-Stokes equations for this phenomenon, almost prohibitively large amount of computational labor is required (Takao 1973). Because at a high Reynolds number, the effect of viscosity is restricted within the thin boundary layer along the surface of the body, the vorticity is assumed to be generated only in that layer. Therefore such a method that can duly treat the vortex motion is desirable. One of such methods is the discrete-vortex approximation, in which the flow field around the body is calculated by replacing the boundary layer with discrete vortices (Kuwahara 1978).

The flow patterns behind the elliptic cylinder with thickness ratio of 0.5 and at the angle of attack of 45° and 90° were studied both numerically by the discrete-vortex approximation and experimentally using the flow visualization techniques, and the comparison of them was made.

2. Numerical simulation

The mechanism of the generation of the vortices is treated as follows: At the instant of impulsive start, the flow field is considered to be inviscid and irrotational, and there is no vorticity in the flow field. However, in order to cancel the velocity slip on the body surface, there must be an infinitely

thin boundary layer along the surface of the cylinder; it is considered as a vortex layer. In the discrete-vortex approximation used, this layer is divided into a finite number of elements, and replaced by the same number of corresponding vortex filaments, the circulations of which are determined to be equal to those of the elements. Computation was carried out using conformal mapping to transform the ellipse (on Z-plane) to a circle (on W-plane). The transformation is given by

$$Z = \frac{1}{2}(aW + 1/(a\cdot\exp(2i\gamma)\cdot W)), \qquad a = \sqrt{3}$$

where γ is the angle of attack. The boundary layer at the initial instant is approximated by 36 vortex filaments, their positions are given by

$$W_j = (1+\varepsilon)\exp(2\pi i(j-\tfrac{1}{2})/2M), \qquad j = 1,\cdots,2M\ ,$$

and their strengths are determined by,

$$\Phi_1 = \Phi_2 = \cdots\cdots = \Phi_{2M}, \qquad \Phi_j = \mathrm{Re}\{f(\exp(2\pi i(j/2M)))\},$$

where 2M is the number of the vortex filaments and f(W) is the velocity potential,

$$f(W) = \frac{a}{2}(W+1/W) + i\sum_{j=1}^{n}\kappa_j \log(W-W_j) - i\sum_{j=1}^{n}\kappa_j \log(W-W_j^*),$$

$$W_j^* = 1/\overline{W}_j.$$

Each point vortex is convected by the velocity field due to the other vortices and their images which are taken in order to match the boundary condition and the initial potential flow. Then after a specified time step, the vortices which have compensated the circulation caused by the initial boundary layer can no longer compensate the new one. Therefore, the new

vortices must be introduced. After the second step, the upper and lower half boundary layers of the cylinder are replaced each by a single vortex filaments, respectively. Larger number of vortex filaments seems desirable, though, considering the fact that the computation time is nearly proportional to the square of the number of the vortex filaments, the number of vortices can not be too large. The least number to acquire a reasonable result is two. The points of generation of the vortices were chosen at the two farthest points on the surface from the center line parallel to the uniform flow. The computed results indicate, however, that the dependence of the flow pattern on the location of the generation points is not so significant, and no special consideration on the position of the nascent vortices is needed. Their strengths are determined similarly to the first step. Repeating these steps, we can get a rotational wake in the frame work of the theory of ideal fluid.

3. Experiment

The elliptic cylinder of 4cm chord length with thickness ratio 0.5 was used for the experiment in a towing tank with impulsive-start capability. Both of aluminum dust method and electrolysis method were used to visualize the stream lines and the streak lines. Motor-driven camera was mounted on the cart which carries the model of elliptic cylinder, and also a video recorder system is adopted for continuous record. Cart speed, U, was varied from 0.5 to 3cm/sec. The Reynolds numbers based on the chord length and this speed were 200 to 1200.

4. Results and Discussion

Figure 1 is an example of the numerical results with an angle of attack of 45° at various times. These are the stream lines and streak lines in the stationary coordinates. Although this method approximates vortex region by singular point vortices, very smooth stream lines of fully developed unsteady wake was obtained within a reasonable computation time. The computation also shows that the position of the nascent vortex need not coincide with the separation point. This is clearly seen on maps of the path lines. [Fig.2] The vortex moves along the cylinder surface to the separation point, and leaves it into the outer flow. The experimental results at the corresponding time to Fig.1 are shown in Fig.3. The drag and lift coefficients [Fig. 4] obtained are generally in good agreement with the values recently reported by Izumi (1980).

In the case of 90°, due to the symmetry, somewhat peculiar process of separation of twin vortices is observed. It is well known that in a moderately low Reynolds number, the Karman street is produced as: the attached eddies stretching farther and farther downstream, become distorted because of small disturbances and then are shed alternatively from the sides of the cylinder. This pattern is well simulated by this approximation. [Fig.5] On the other hand, in a higher Reynolds number, the secondary vortices appear just behind the separation point, and, with the growth of these secondary vortices, and with their intrusion into the region between the elliptic cylinder and twin vortices, the initial twin vortices separate suddenly from the

cylinder symmetrically if asymmetrical disturbances are carefully reduced.

In order to see this separation process it is essential to take into account of the effect of the backward flow due to the twin vortices just behind the cylinder, then at least four vortex filaments must be introduced after the second step, two for front boundary layer, two for rear boundary layer. The flow patterns thus obtained are shown in Fig.6, in which sudden separation process of twin vortices is well simulated. The corresponding experimental results are shown in Fig.7.

The relation of the length of the twin vortices to the non-dimensional time $T = Ut/a$, where a is the chord length, are plotted in Fig.8 for various Reynolds numbers. The agreement between the measured and the numerical results is excellent.

References

Izumi, K. 1980 ERC Rept. Univ. Tsukuba, vol.4.
Kuwahara, K. 1978 J. Phys. Soc. Japan, vol.45
Takao, Y. 1973 Japan IBM Sci. Center Rept., G318-1909-0.

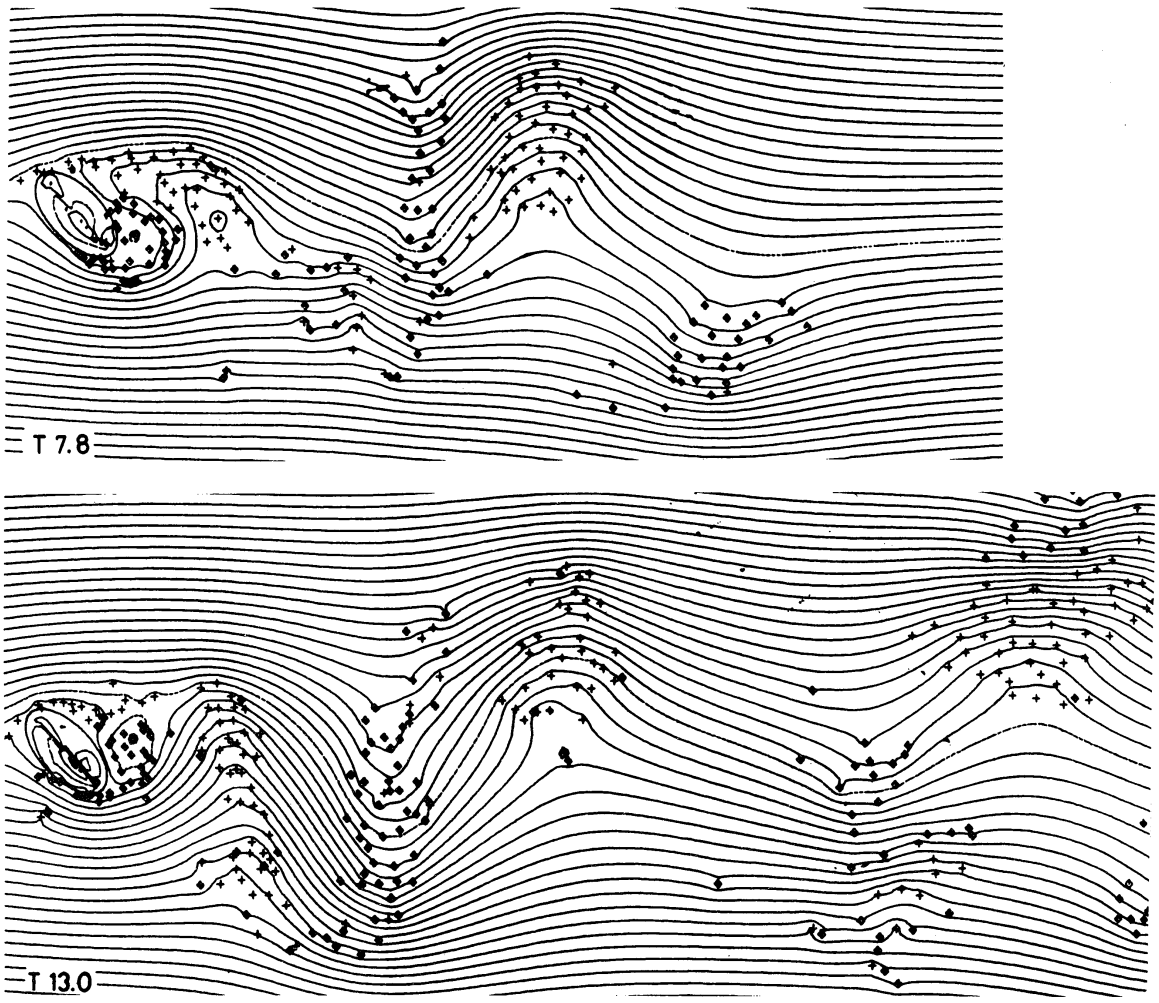

Fig.1 Vortex arrangements and stream lines (45°).
Mark + and ◇ are vortex filaments with clockwise and counter-clockwise rotations respectively.

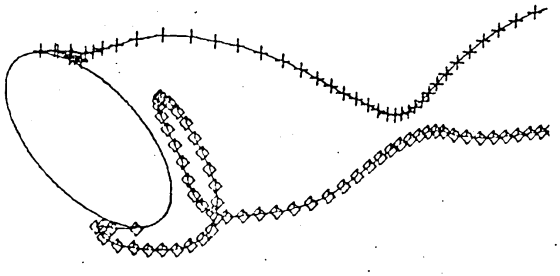

Fig.2 Particle paths (45°).

Fig.3 Stream lines (45°);
Experiment, T = 7.8.

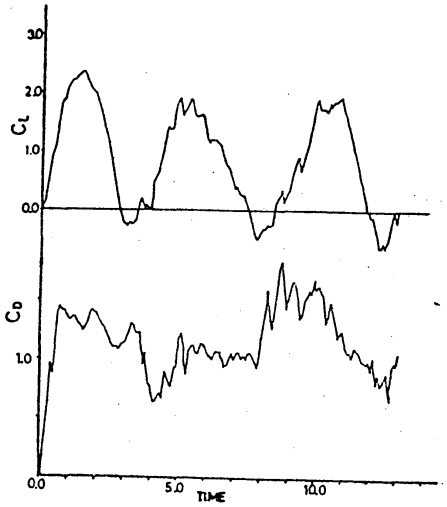

Fig.4 Drag and lift coefficients (45°).

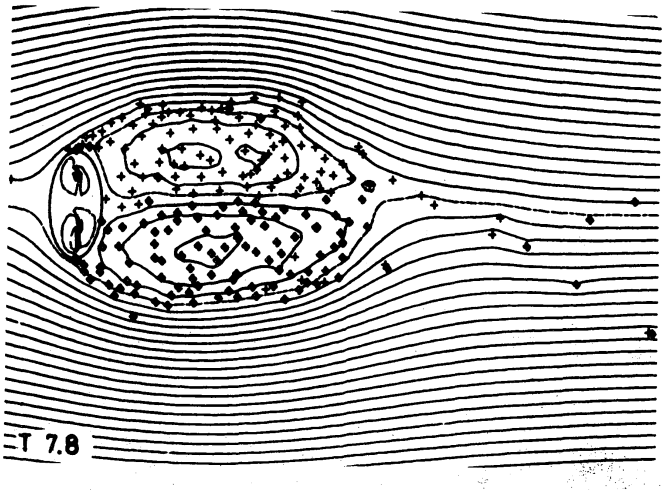

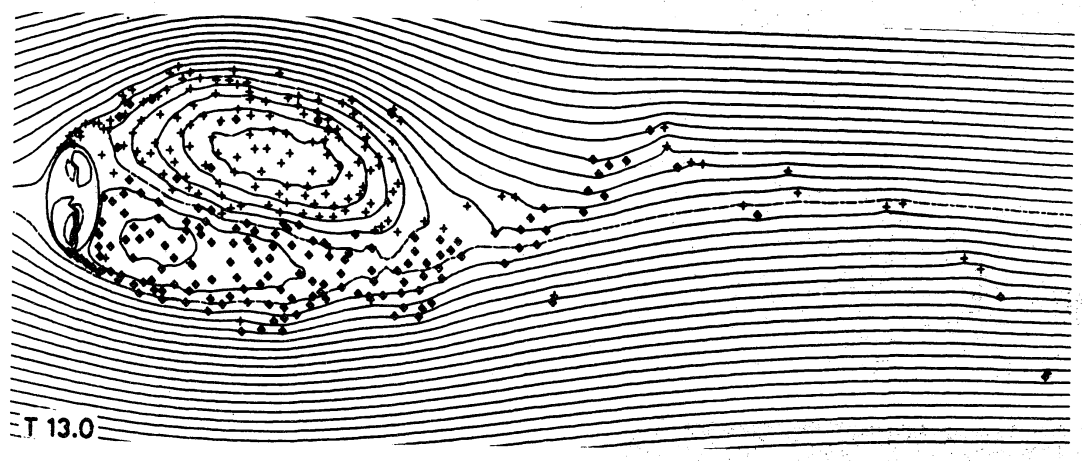

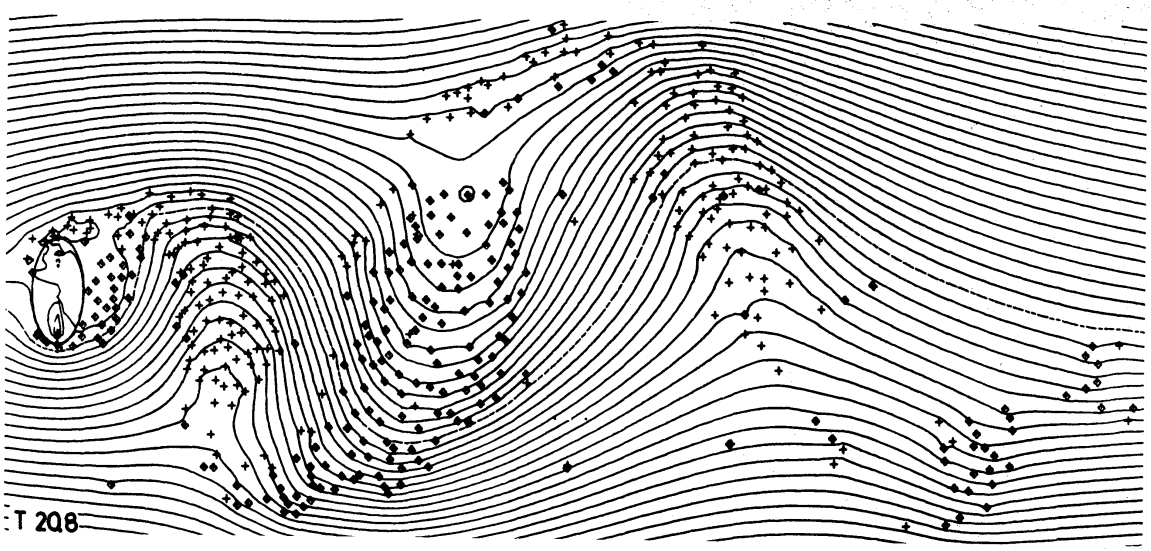

Fig.5 Vortex arrangements and stream lines(90°). Simpler case.

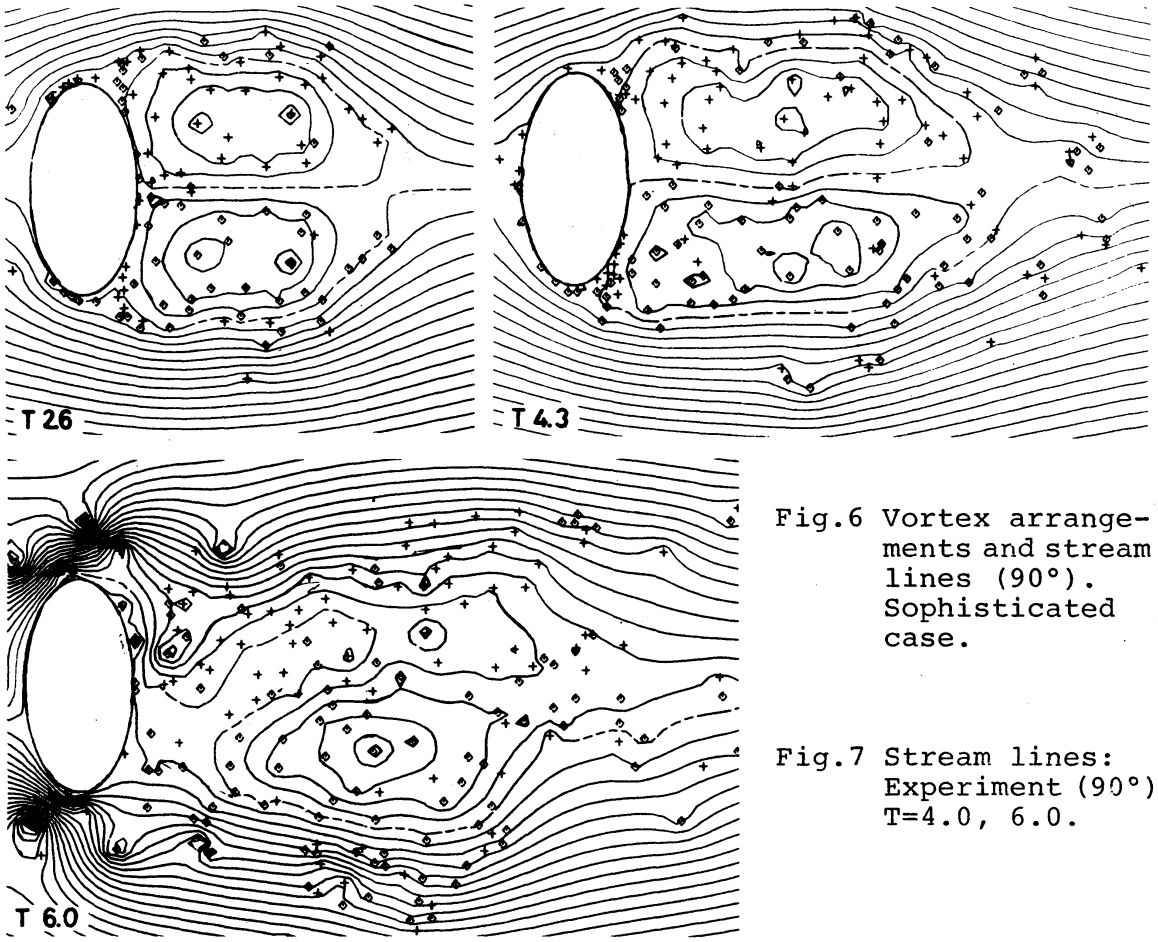

Fig.6 Vortex arrangements and stream lines (90°). Sophisticated case.

Fig.7 Stream lines: Experiment (90°), T=4.0, 6.0.

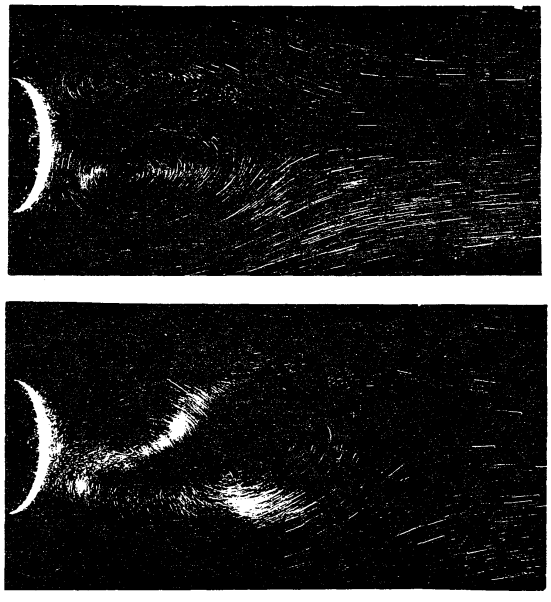

Fig.7

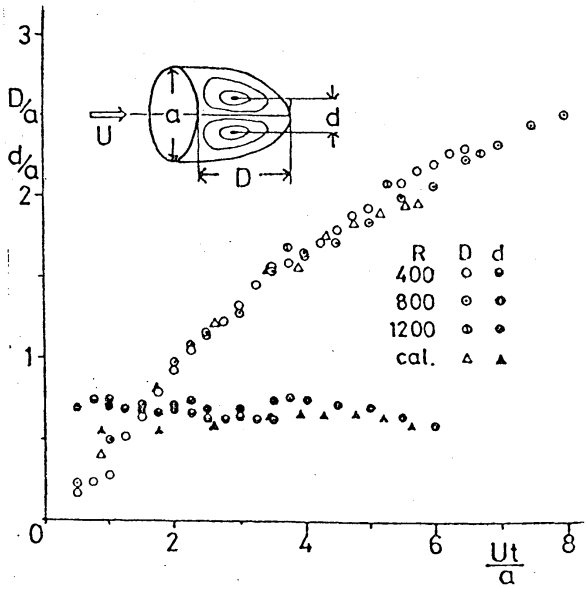

Fig.8 Length of twin vortices.

PART II OSCILLATING AIRFOIL

1. Introduction

An oscillating airfoil in pitch and/or in heave with its maximum angle of attack larger than the static stall one, experiences peculiar hysteresis in drag, lift and moment coefficients. It is believed that these phenomena are caused by the formation of the leading edge separation vortex, its convection along the wing surface and its shedding into the wake (Carr et al., 1977).

The linearized unsteady airfoil theory has been widely used for the analysis of the smaller amplitude oscillation than the dynamic stall angle. It was first developed by Theodorsen(1935) and Karman & Sears (1938) and was improved since then by including the airfoil thickness and the wake deformation etc. However in order to treat the dynamic stall, the unsteady separated flow theory is needed.

The flow field around an oscillating NACA0012 airfoil in pitch was analyzed by solving numerically the two dimensional Navier-Stokes equations for fairly large Reynolds numbers (Mehta 1977). In this calculation the process of the dynamic stall was clearly presented. But this calculation was quite computer-time consuming. The leading edge separation was taken into account by Ham(1968) in the potential theory, in which the strength of the shedded vortex was determined using the Kutta condition at the leading edge and the trailing edge. But some phenomenological argument based on experiments was needed, and the

satisfactory results were not obtained.

In the present analysis the boundary layer formed on the surface of the wing was replaced by a finite number of discrete vortices at each time step and their interactions were calculated to determine their convected positions. Thus the process of formation and convection of separated flow mass could be simulated. In order to determine the strength of newly generated vortices, the "Non-Slip" condition was introduced instead of the usual Kutta condition (Kuwahara 1978). So this theory could be applied to the analysis of the dynamic stall without further assumptions.

2. Mathematical Formulation

Let us consider a two dimensional NACA airfoil (its chord length 4a) oscillating in pitch and/or in heave. The pitching angle α (positive in the clockwise rotation) and the vertical displacement of the pitching axis Y_h (assumed on the Y-axis) vary following the next formulae:

$$\alpha = \alpha_0 - \bar{\alpha}\cos\omega t, \qquad Y_h = H\sin(\omega t + \beta). \tag{1}$$

where β is arbitrary (Fig. 1). The flow field around the oscillating airfoil (z-plane) is conformally mapped outside the static unit circle (ζ-plane) by the following transformations: (Fig. 2)

$$z = \left[a'\left(\zeta + \gamma + \frac{c^2}{\zeta+\gamma}\right) - b\right]e^{-i\alpha} + iY_h = G(\zeta,t), \tag{2}$$

$$\gamma = \xi_0 + i\eta_0,$$
$$c = (\xi_0 + (1-\eta_0^2)^{\frac{1}{2}}(1-\delta). \qquad (3)$$

Parameters a', c, b, ξ_0, δ are determined according to Mehta (1977).

Laplace equation must be solved under the boundary condition that the normal component of the difference between the velocity of the body surface $(\dot{X},\dot{Y})$ and that of the fluid particle attached to it (u,v) is zero: (Fig. 3)

$$(u-\dot{X})\cdot\cos\theta + (v-\dot{Y})\cdot\sin\theta = 0. \qquad (4)$$

On the unit circle in the ζ-plane it is represented as

$$\mathrm{Re}[\zeta\cdot F_\zeta] = \mathrm{Re}[\zeta\cdot G_\zeta\cdot\bar{G}_t], \qquad |\zeta|=1. \qquad (5)$$

So the complex potential at time step N is as follows:

$$F = a'u(\zeta e^{-i\alpha}+e^{i\alpha}/\zeta) + i\dot{\alpha}a'^2(A/\zeta+B/(\zeta+\gamma))$$
$$- i\dot{Y}_h a'(e^{i\alpha}/\zeta+c^2e^{-i\alpha}/(\zeta+\gamma))$$
$$+ i\sum_{j=1}^{N}\sum_{k=1}^{M}\kappa^{jk}(\ln(\zeta-\zeta^{jk}) - \ln(\zeta-1/\bar{\zeta}^{jk})), \qquad (6)$$

$$A = \gamma - b/a' + c^2/\gamma, \quad B = c^2(\gamma-1/\gamma) - bc^2/a + c^4\gamma/(\gamma^2-1),$$

where M is the number of discrete vortices generated at each time step and ζ^{jk} is the location of the k-th vortex genarated at time step j.

The "Non-Slip" condition is introduced to determine the strength of vortices. The non-slip condition for the viscous fluid is represented as

$$(u-\dot{X})\cdot\sin\theta - (v-\dot{Y})\cdot\cos\theta = 0. \qquad (7)$$

It is also expressed on the unit circle in the ζ-plane as follows:

$$\mathrm{Im}(\zeta \cdot F_\zeta) = \mathrm{Im}(\zeta \cdot G_\zeta \cdot \overline{G}_t), \qquad |\zeta|=1. \qquad (8)$$

Within the framework of discrete-vortex approximation, it is impossible to satisfy eq.(8) on the entire circle. So by integrating eq.(8) along the unit circle, the following equation is obtained for the velocity potential Φ:

$$\Phi_{k+1} - \Phi_k = -\int_{\theta_k}^{\theta_{k+1}} \mathrm{Im}(\zeta \cdot G_\zeta \cdot \overline{G}_t) d\theta, \qquad (9)$$

$$\theta_k = \arg(\zeta_k). \qquad (10)$$

Eq.(9) means that no net flow exists on the average sense along the wing surface between two points ζ_k and ζ_{k+1}. This is why eq.(9) is called the "Non-Slip" condition. In order to fulfill eq.(9), a discrete vortex is generated just outside the unit circle between ζ_k and ζ_{k+1} at each time step (Fig. 4).

The induced velocity of the k-th vortex generated at time step j is as follows:

$$\frac{dz^{jk}}{dt} = \left(\overline{\frac{dF^{jk}}{dz}} \right)_{z=z^{jk}}, \qquad (11)$$

$$F^{jk} = F - i\kappa^{jk} \ln(\zeta - \zeta^{jk}). \qquad (12)$$

So in the ζ-plane it is represented as

$$\frac{d\zeta^{jk}}{dt} = \left[\left(\overline{\frac{dF^{jk}}{d\zeta}} \cdot \frac{d\zeta}{dz} \right) - \frac{dz}{dt} \right) \cdot \frac{d\zeta}{dz} \Big]_{\zeta=\zeta^{jk}}. \qquad (13)$$

The new convected position is determined at time $t_{N+1}=t_N+\Delta t$ with the following equations:

$$\zeta_{N+1}^{jk} = \zeta_N^{jk} + \left(\frac{d\zeta^{jk}}{dt} \right)_N \cdot \Delta t. \qquad (14)$$

The drag D, the lift L, and the moment M are calculated using the following formulae:

$$D - iL = -i \oint p \, d\bar{z},$$

$$M = -\frac{1}{2} \mathrm{Re}\left[\oint p\bar{z} \, dz\right], \qquad (15)$$

$$p = p_0(t) - \frac{\partial \Phi}{\partial t} - \frac{1}{2} \frac{dF}{dz} \left(\frac{\overline{dF}}{dz} \right).$$

3. Results

Numerical calculations were carried out chiefly for the pitching oscillation of α_0=10°-15°, $\bar{\alpha}$=10°-15°. The reduced frequency $K=\omega(2a)/U$ was 0.125-2.45. The airfoil surface was divided into two parts, one was the forward half and the other was the rear half of the wing. Two discrete vortices were generated near the leading edge and the trailing edge. The computer used was HITAC-8700 at Nihon Univ.

In Fig. 5 the vortex distribution and the instantaneous streamlines are shown on the case K=2.45. TIME means t/T, in which t is the elapsed time from the beginning of the oscillation and T is the period of the oscillation. The process of the formation of the leading edge separation vortex, its convection along the wing surface and its shedding into the wake is clearly demonstrated. The reattaching process near the leading edge is also shown.

In Fig. 6 drag, lift and moment coefficients versus the angle of attack α are shown for the case K=0.5 and 0.25. The

results of the linearized theory are also shown by dotted lines. When the angle of attack α is small, the difference between the calculated results and those of the linearized theory is small. But when α is large, their fluctuations become remarkable and their discrepancy is significant. Judging from the instantaneous streamlines, the leading edge separation bubbles were formulated in both cases, but in the case K=0.5, the lift stall does not occur, though in the case K=0.25, the sharp dynamic stall of lift takes place. This is probably because when the reduced frequency is large, the growth of the leading edge separation vortex is not sufficient on account of the quick decrease of the angle of attack.

4. Conclusion

The unsteady separated flow theory by the discrete-vortex approximation was developed and was applied to the flow field of an oscillating airfoil in pitch and/or in heave. The process of the formation of the leading edge separation vortex, its convection along the wing surface and its shedding into the wake was presented. When the reduced frequency defined with the half chord length was larger than 0.5, the lift stall did not occur. On the contrary when K was less than 0.25, the sharp lift stall curve was obtained.

References

Carr, L.W., McAlister, K.W. & McCroskey, W.G. 1977 NASA TND-8382.
Ham, N.D. 1968 AIAA Journal, vol.6, No.10.
von Karman, T. & Sears, W.R. 1938 J. Aero. Sci., vol.5, No.10.
Kuwahara, K. 1978 J. Phys. Soc. Japan vol.45.
Mehta, U.B. 1977 AGARD Paper 23.
Theodorsen, T. 1935 NACA Report 496.

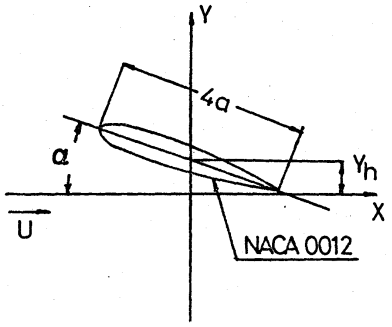

Fig. 1 A reference of frame in the physical plane (z-plane)

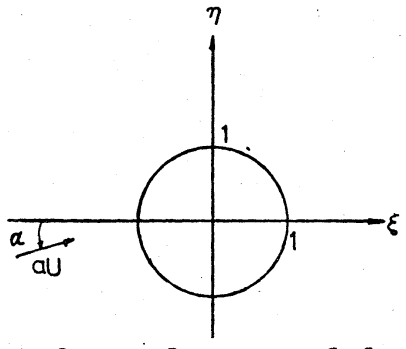

Fig. 2 A reference of frame in the mapped plane (ζ-plane)

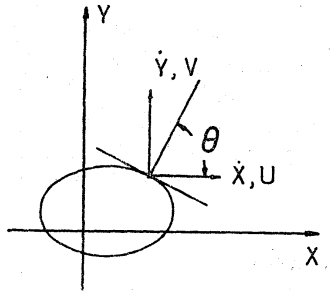

Fig. 3 The definition of u,v, $\dot{X},\dot{Y}$ and θ.

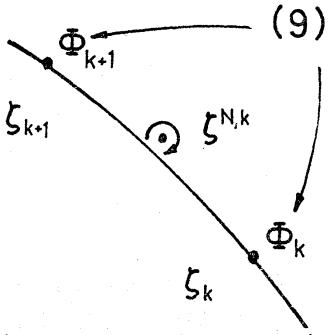

Fig. 4 The "Non-Slip" condition

(a) TIME = 1.0

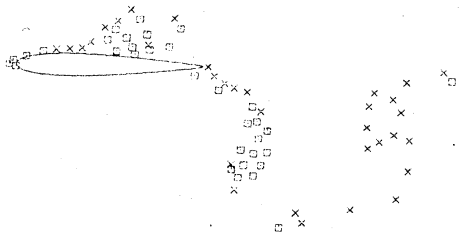

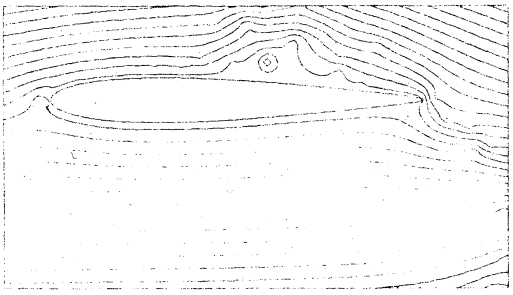

(b) TIME = 1.25

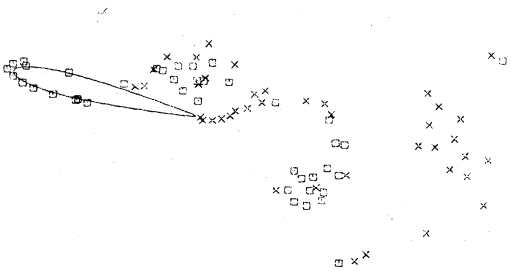

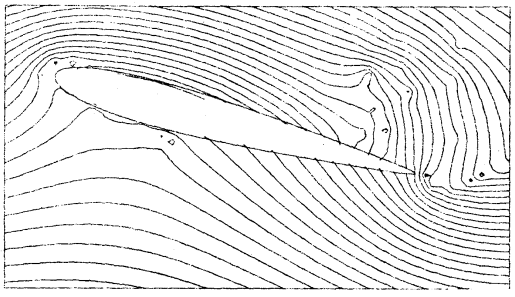

(to be continued)

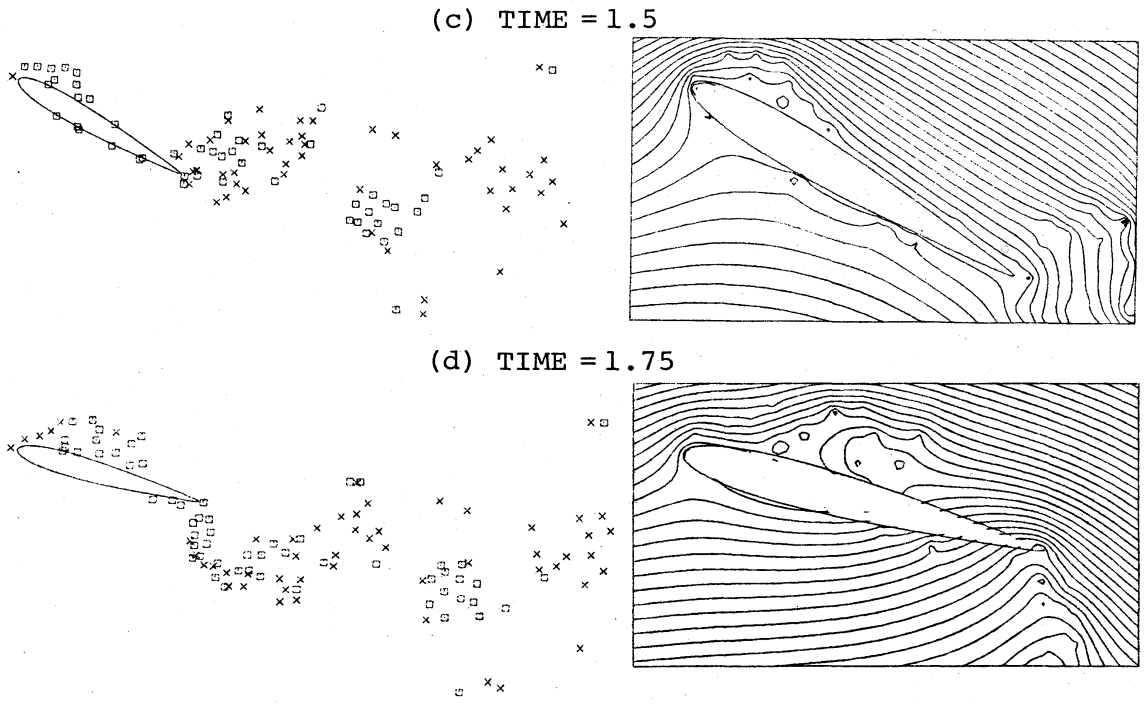

□ A vortex with clockwise rotation
× A vortex with counter-clockwise rotation

Fig. 5 The vortex distribution and the instantaneous streamlines (U=2cm/s, T=2.56s, 4a=4cm, $\alpha=15°-15°\cos\omega t$, K=2.45, TIME=t/T)

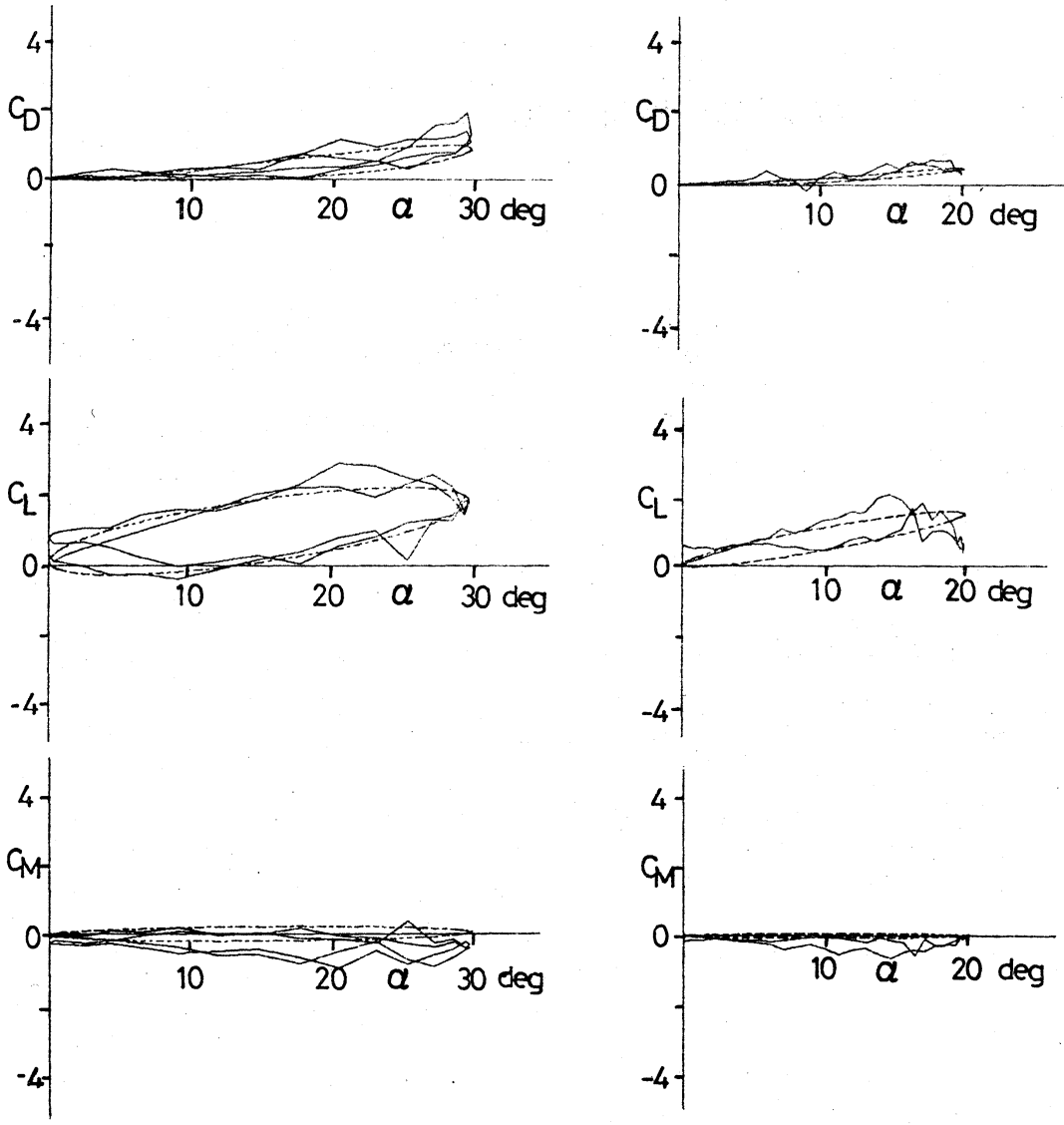

(U=25cm/s, T=1s, 4a=4cm, α=15°-15°cosωt, K=0.5)

(U=25cm/s, T=2s, 4a=4cm, α=10°-10°cosωt, K=0.25)

Fig. 6 The drag, lift and moment coefficients versus the angle of attack.